

Chapter 26

Universality in transitions to chaos

The developments that we shall describe next are one of those pleasing demonstrations of the unity of physics. The key discovery was made by a physicist not trained to work on problems of turbulence. In the fall of 1975 Mitchell J. Feigenbaum, an elementary particle theorist, discovered a universal transition to chaos in one-dimensional unimodal map dynamics. At the time the physical implications of the discovery were nil. During the next few years, however, numerical and mathematical studies established this universality in a number of realistic models in various physical settings, and in 1980 the universality theory passed its first experimental test.

The discovery was that large classes of nonlinear systems exhibit transitions to chaos which are *universal* and *quantitatively* measurable. This advance was akin to (and inspired by) earlier advances in the theory of phase transitions; for the first time one could, predict and measure “critical exponents” for turbulence. But the breakthrough consisted not so much in discovering a new set of universal numbers, as in developing a new way to solve strongly nonlinear physical problems. Traditionally, we use regular motions (harmonic oscillators, plane waves, free particles, etc.) as zeroth-order approximations to physical systems, and account for weak nonlinearities perturbatively. We think of a dynamical system as a smooth system whose evolution we can follow by integrating a set of differential equations. The universality theory tells us that the zeroth-order approximations to strongly nonlinear systems should be quite different. They show an amazingly rich structure which is not at all apparent in their formulation in terms of differential equations; instead, they exhibit self-similar structures which can be encoded by universality equations of a type which we will describe here. To put it more provocatively: junk your old equations and look for guidance in clouds’ repeating patterns.

In this chapter we reverse the chronology, describing first a turbulence experiment, then a numerical experiment, and finally explain the observations using the universality theory. We will try to be intuitive and concen-

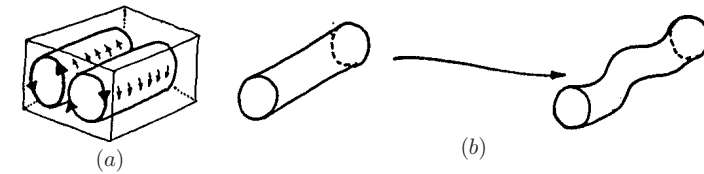


Figure 26.1:

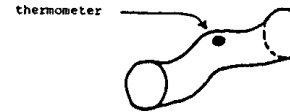


Figure 26.2:

trate on a few key ideas. Even though we illustrate it by onset of turbulence, the universality theory is by no means restricted to the problems of fluid dynamics.

26.1 Onset of turbulence

We start by describing schematically the 1980 experiment of Libchaber and Maurer. In the experiment a liquid is contained in a small box heated from the bottom. The salient points are:

1. There is a *controllable parameter*, the Rayleigh number, which is proportional to the temperature difference between the bottom and the top of the cell.
2. The system is *dissipative*. Whenever the Rayleigh number is increased, one waits for the *transients to die out*.
3. The container, figure 26.1(a), has a small “aspect ratio”; its width is a small integer multiple of its height, approximately.

For small temperature gradients there is a heat flow across the cell, but the liquid is static. At a critical temperature a convective flow sets in. The hot liquid rises in the middle, the cool liquid flows down at the sides, and two convective rolls appear. So far everything is as expected from standard bifurcation scenarios. As the temperature difference is increased further, the rolls become unstable in a very specific way - a wave starts running along the roll, figure 26.1(b).

As the warm liquid is rising on one side of the roll, while cool liquid is descending down the other side, the position and the sideways velocity of the ridge can be measured with a thermometer, figure 26.2. One observes a sinusoid, figure 26.3. The periodicity of this instability suggests two other ways of displaying the measurement, figure 26.4.

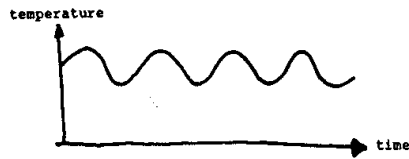


Figure 26.3:

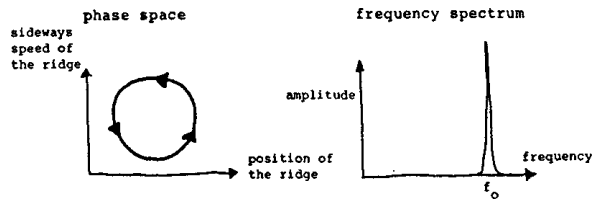


Figure 26.4:

Now the temperature difference is increased further. After the stabilization of the phase-space trajectory, a new wave is observed superimposed on the original sinusoidal instability. The three ways of looking at it (real time, phase space, frequency spectrum) are sketched in figure 26.5. A coarse measurement would make us believe that T_0 is the periodicity. However, a closer look reveals that the phase-space trajectory misses the starting point at T_0 , and closes on itself only after $2T_0$. If we look at the frequency spectrum, a new wave band has appeared at half the original frequency. Its amplitude is small, because the phase-space trajectory is still approximately a circle with periodicity T_0 .

As one increases the temperature very slightly, a fascinating thing happens: the phase-space trajectory undergoes a very fine splitting, see figure 26.6. We see that there are three scales involved here. Looking casually, we see a circle with period T_0 ; looking a little closer, we see a pretzel with period $2T_0$; and looking very closely, we see that the trajectory closes on itself only after $4T_0$. The same information can be read off the frequency

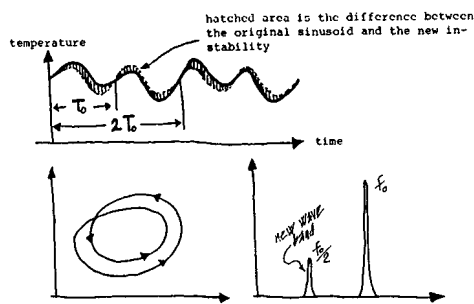


Figure 26.5:

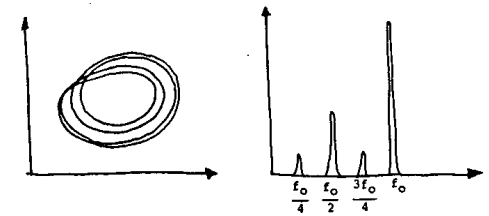


Figure 26.6:

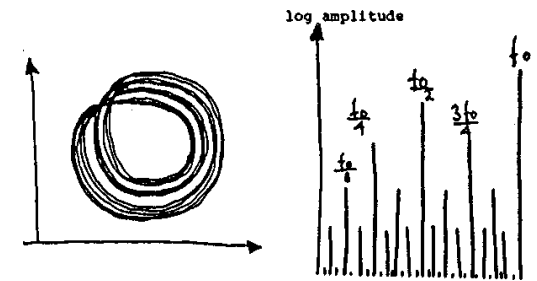


Figure 26.7:

spectrum; the dominant frequency is f_0 (the circle), then $f_0/2$ (the pretzel), and finally, much weaker $f_0/4$ and $3f_0/4$.

The experiment now becomes very difficult. A minute increase in the temperature gradient causes the phase-space trajectory to split on an even finer scale, with the periodicity $2^3 T_0$. If the noise were not killing us, we would expect these splittings to continue, yielding a trajectory with finer and finer detail, and a frequency spectrum of figure 26.7, with families of ever weaker frequency components. For a critical value of the Rayleigh number, the periodicity of the system is $2^\infty T_0$, and the convective rolls have become turbulent. This *weak turbulence* is today usually referred to as the “onset of chaos”. Globally, the rolls persist but are wiggling irregularly. The ripples which are running along them show no periodicity, and the spectrum of an idealized, noise-free experiment contains infinitely many subharmonics, figure 26.8. If one increases the temperature gradient

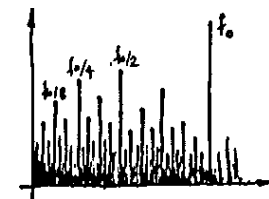


Figure 26.8:

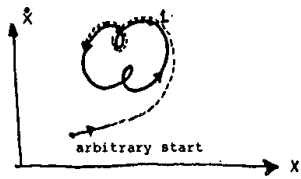


Figure 26.9:

beyond this critical value, there are further surprises (see, for example, figure 26.16) which we will not discuss here.

We now turn to a numerical simulation of a simple nonlinear oscillator in order to start understanding why the phase-space trajectory splits in this peculiar fashion.

26.2 Onset of chaos in a numerical experiment

In the experiment that we have just described, limited experimental resolution makes it impossible to observe more than a few bifurcations. Much longer sequences can be measured in numerical experiments. A typical example is the nonlinear Duffing oscillator

$$\ddot{x} + \gamma\dot{x} - x + 4x^3 = A \cos(\omega t). \tag{26.1}$$

The oscillator is driven by an external force of frequency ω , with amplitude A period $T_0 = 2\pi/\omega$. The dissipation is controlled by the friction coefficient γ . (See (2.6) and example 5.1.) Given the initial displacement and velocity one can easily follow numerically the state phase-space trajectory of the system. Due to the dissipation it does not matter where one starts; for a wide range of initial points the phase-space trajectory converges to an attracting *limit cycle* (trajectory loops onto itself) which for some $\gamma = \gamma_0$ looks something like figure 26.9. If it were not for the external driving force, the oscillator would have simply come to a stop. As it is, executing a motion forced on it externally, independent of the initial displacement and velocity. Starting at the point marked 1, the pendulum returns to it after the unit period T_0 .

However, as one decreases, the same phenomenon is observed as in the turbulence experiment; the limit cycle undergoes a series of period-doublings, figure 26.10. The trajectory keeps on nearly missing the starting point, until it hits exactly $2^n T_0$. The phase-space trajectory is getting increasingly hard to draw; however, the sequence of points 1, 2, ..., 2^n , which corresponds to the state of the oscillator at times $T_0, 2T_0, \dots, 2^n T_0$, sits in a small region of the phase space, so in figure 26.11 we enlarge it for a closer look. Globally the trajectories of the turbulence experiment

Duffing!damped

cite_Arecchi and Lisi (1982)
 26.2
 page 542

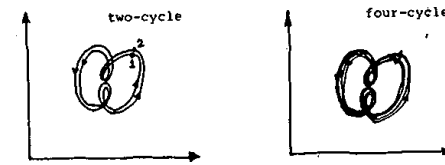


Figure 26.10:

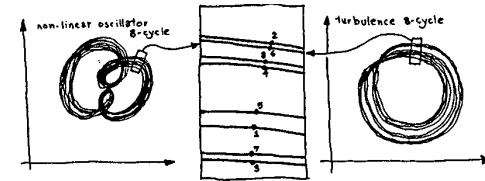


Figure 26.11:

and of the non-linear oscillator numerical experiment look very different. However, the above sequence of near misses is *local*, and looks roughly the same for both systems. This sequence of points lies approximately on a straight line, figure 26.12. Let us concentrate on this line, reducing the dimensionality of the phase space by a Poincaré map. The Poincaré map contains all the information we need; from it we can read off when an instability occurs, and how large it is. One varies continuously the non-linearity parameter (friction, Rayleigh number, etc.) and plots the location of the intersection points; in the present case, the Poincaré surface is - for all practical purposes - a smooth 1-dimensional curve, and the result is a *bifurcation tree* of figure 26.13. We already have some *qualitative* understanding of this plot. The phase-space trajectories we have drawn are localized (the energy of the oscillator is bounded) so the tree has a finite span. Bifurcations occur simultaneously because we are cutting a single trajectory; when it splits, it does so everywhere along its length. Finer and finer scales characterize both the branch separations and the branch lengths.

Feigenbaum's discovery consists of the following *quantitative* observations:



Figure 26.12:

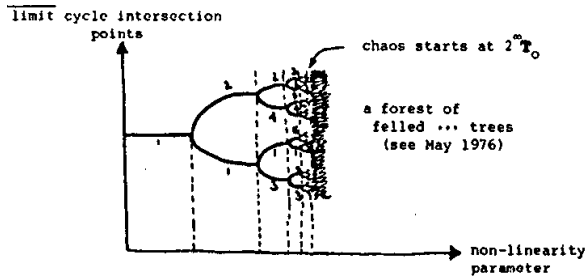


Figure 26.13:

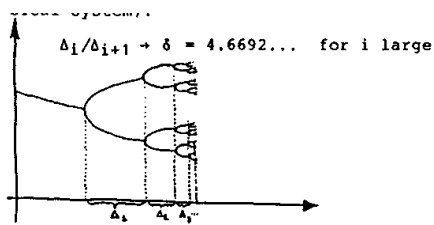


Figure 26.14:

1. The *parameter convergence* is universal (i.e., independent of the particular physical system), $\Delta_i/\Delta_{i+1} \rightarrow 4.6692\dots$ for i large, see figure 26.14.
2. The relative scale of successive *branch splittings* is universal: $\epsilon_i/\epsilon_{i+1} \rightarrow 2.5029\dots$ for i large, see figure 26.15.

The beauty of this discovery is that if turbulence (chaos) is arrived at through an infinite sequence of bifurcations, we have two quantitative predictions:

1. The convergence of the critical Rayleigh numbers corresponding to the cycles of length 2, 4, 8, 16, ... is controlled by the universal convergence parameter $\delta = 4.6692016\dots$

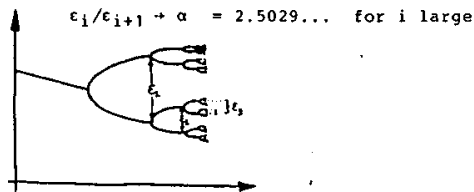
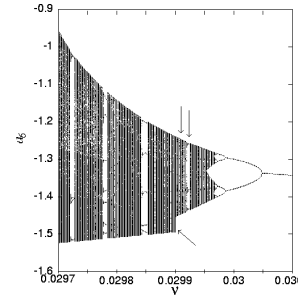


Figure 26.15:

period-doubling!tree

Figure 26.16: A period-doubling tree observed in a small size Kuramoto-Sivashinsky system, generated under adiabatic change of the damping parameter (system size). The choice of projection down to the coordinate a_6 is arbitrary; projected down to any coordinate, the tree is qualitatively the same. The two upper arrows indicate typical values: for $\nu = 0.029910$ dynamics appears chaotic, and $\nu = 0.029924$ there is a “golden-mean” repelling set coexisting with attractive period-3 window. The lower arrow indicates the value at which upper invariant set with this merges with its $u(x) \rightarrow -u(-x)$ symmetry partner. $N = 16$ Fourier modes truncation of (25.8). Truncation to $N = 17$ modes yields a similar figure, with values for specific bifurcation points shifted by $\sim 10^{-5}$ with respect to the $N = 16$ values. (from ref. [25.4])



2. The splitting of the phase-space trajectory is controlled by the universal scaling parameter $\alpha = 2.50290787\dots$. As we have indicated in our discussion of the turbulence experiment, the relative heights of successive subharmonics measure this splitting and hence α .

↓PRELIMINARY

These universal numbers are measured in a variety of experiments: a sample of early experiments is given in table ?.

↑PRELIMINARY

While this universality was derived through study of simple, few-dimensional systems (pendulum, oscillations along a convective roll), it also applies to high- or even infinite-dimensional systems, such as. discretizations of the Navier-Stokes equations, and in the literature there are innumerable other examples of period-doublings in many-dimensional systems. A wonderful thing about this universality is that it does not matter much how close our equations are to the ones chosen by nature; as long as the model is in the same universality class (in practice this means that it can be modeled by a mapping of form (26.2)) as the real system, both will undergo a period-doubling sequence. That means that we can get the right physics out of very simple models, and this is precisely what we will do next.

Example 26.1 Period doubling tree in a flame flutter. For $\nu > 1$, $u(x, t) = 0$ is the globally attractive stable equilibrium; starting with $\nu = 1$ the solutions go through a rich sequence of bifurcations.

Figure 26.16 is a representative plot of the period-doubling tree for the Poincaré map P . To obtain this figure, we took a random initial point, iterated it for a some time to let it settle on the attractor and then plotted the a_6 coordinate of the next 1000 intersections with the Poincaré section. Repeating this for different values of the damping parameter ν , one can obtain a picture of the attractor as a function of ν ; the dynamics exhibits a rich variety of behaviors, such as strange attractors, stable limit cycles, and so on.

use Holmes-Lumley discussion might prefer articles/vachtang/feig16.ps



Figure 26.17:

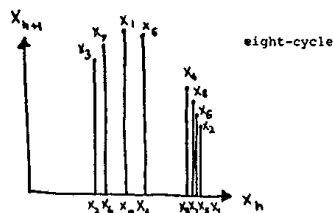


Figure 26.18:

The reason why multidimensional *dissipative* systems become effectively one-dimensional is that: for a dissipative system phase-space volumes shrink. They shrink at different rates in different directions, as in figure 26.17. The direction of the slowest convergence defines a one-dimensional line which will contain the attractor (the region of the phase space to which the trajectory is confined at asymptotic times):

What we have presented so far are a few experimental facts; we now have to convince you that they are universal.

26.3 What does all this have to do with fishing?

Looking at the phase-space trajectories shown earlier, we observe that the trajectory bounces within a restricted region of the phase space. How does this happen? One way to describe this bouncing is to plot the $(n+1)$ th intersection of the trajectory with the Poincaré surface as a function of the preceding intersection. Referring to figure 26.12 we find the map of figure 26.18. This is a Poincaré return map for the limit cycle. If we start at various points in the phase space (keeping the non-linearity parameter fixed) and mark all passes as the trajectory converges to the limit cycle, we trace an approximately continuous curve $f(x)$ of figure 26.19. which gives the location of the trajectory at time $t + T_0$ as a function of its location at time t :

$$x_{n+1} = f(x_n), \tag{26.2}$$

The trajectory bounces within a trough in the phase space, and $f(x)$ gives a local description of the way the trajectories converge to the limit cycle. In principle we know $f(x)$, as we can measure it (see Simoyi, Wolf and Swinney (1982) for a construction of a return map in a chemical turbulence

↓PRELIMINARY

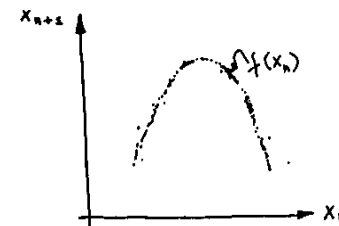


Figure 26.19:

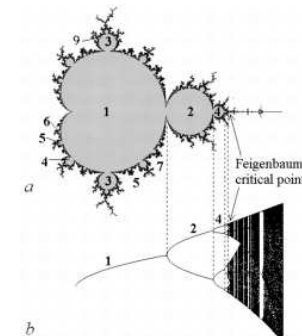


Figure 26.20: Correspondence between (a) the Mandelbrot set, shown in plane $(\text{Re}\lambda, \text{Im}\lambda)$ for the map $z_{k+1} = \lambda - z_k^2$, and (b) the period-doubling bifurcation tree plane (λ, x) , $x, \lambda \in \mathbb{R}$. (from ref. [26.14])

experiment, or compute it from the equations of motion. The form of $f(x)$ depends on the choice of Poincaré map, and an analytic expression for $f(x)$ is in general not available (see Gonzales and Piro (1983) for an example of an explicit return map), but we know what $f(x)$ should look like; it has to fall on both sides (to confine the trajectory), so it has a maximum. Around the maximum it looks like a parabola

$$f(x) = a_0 + a_2(x - x_c)^2 + \dots \tag{26.3}$$

ask for permission to use figure 26.20 like any sensible polynomial approximation to a function with a hump.

This brings us to the problem of a rational approach to fishery. By means of a Poincaré map we have reduced a continuous trajectory in phase space to one-dimensional iteration. This one-dimensional iteration is studied in population biology, where $f(x)$ is interpreted as a population curve (the number of fish x_{n+1} in the given year as a function of the number of fish x_n the preceding year), and the bifurcation tree figure 26.13 has been studied in considerable detail.

The first thing we need to understand is the way in which a trajectory converges to a limit cycle. A numerical experiment will give us something like figure 26.21. In the Poincaré map the limit trajectory maps onto itself, $x^* = f(x^*)$. Hence a limit trajectory corresponds to a *fixed point* of $f(x)$. Take a programmable pocket calculator and try to determine x^* . Type in

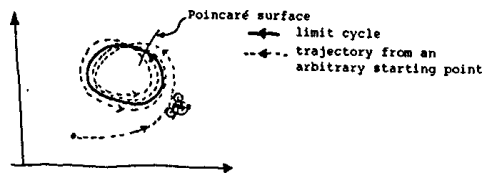


Figure 26.21:

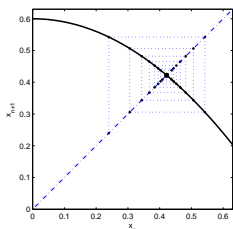


Figure 26.22:

a simple approximation to $f(x)$, such as

$$f(x) = \lambda - x^2. \tag{26.4}$$

Here λ is the non-linear parameter. Enter your guess x_0 and press the button. The number x_1 appears on the display. Is it a fixed point? Press the button again, and again, until $x_{n+1} = x_n$ to desired accuracy. Diagrammatically, this is illustrated by the web traced out by the trajectory in figure 26.22. Note the tremendous simplification gained by the use of the Poincaré map. Instead of computing the entire phase-space trajectory by a numerical integration of the equations of motion, we are merely pressing a button on a pocket calculator.

This little calculation confirms one's intuition about fishery. Given a fishpond, and sufficient time, one expects the number of fish to stabilize. However, no such luck - a rational fishery manager soon discovers that anything can happen from year to year. The reason is that the fixed point x^* need not be attractive, and our pocket calculator computation need not converge.

26.4 A universal equation

Why is the naive fishery manager wrong in concluding that the number of fish will eventually stabilize? He is right when he says that $x^* = f(x^*)$ corresponds to the same number of fish every year. However, this is not necessarily a stable situation. Reconsider how we got to the fixed point in

universal function \rightarrow
universal fixed-point
function?

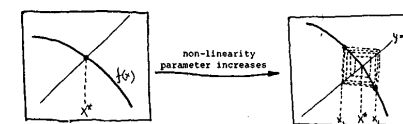


Figure 26.23:

figure 26.22. Starting with a sufficiently good guess, the iterates converge to the fixed point. Now start increasing gently the non-linearity parameter (Rayleigh number, the nutritional value of the pond, etc.). $f(x)$ will slowly change shape, getting steeper and steeper at the fixed point, until the fixed point becomes unstable and gives birth to a cycle of two points. This is precisely the first bifurcation observed in our experiments.

Example 26.2 Fixed point stability.

The fixed point condition for map (26.4) $x^2 + x - \lambda = 0$ yields 2 fixed points.

$$x_{pm} = \frac{-1 \pm \sqrt{1 + 4\lambda}}{\text{what?}}$$

The fixed point x_+ loses stability at $\lambda = -1$. Inserted into $\lambda = f'(x) = -2x$, this yields

$$\lambda = 3/4, \quad x_+ = 1/2$$

as the value at which fixed point x_+ loses stability.

This is the only gentle way in which our trajectory can become unstable (cycles of other lengths can be created, but that requires delicate fiddling with parameters; such bifurcations are not generic). Now we return to the same point after every second iteration

$$x_i = f(f(x_i)), \quad i = 1, 2.$$

so the cycle points of $f(x)$ are the fixed points of $f(f(x))$.

To study their stability, we plot $f(f(x))$ alongside $f(x)$ in figure 26.24. What happens as we continue to increase the "Rayleigh number"? $f(x)$ becomes steeper at its fixed point, and so does $f(f(x))$. Eventually the magnitude of the slope at the fixed points of $f(f(x))$ exceeds one, and they bifurcate. Now the cycle is of length four, and we can study the stability of the fixed points of the fourth iterate. They too will bifurcate, and so forth. This is why the phase-space trajectories keep on splitting $2 \rightarrow 4 \rightarrow 8 \rightarrow 16 \rightarrow 32 \dots$ in our experiments. The argument does not depend on the precise form of $f(x)$, and therefore the phenomenon of successive period-doublings is *universal*.

More amazingly, this universality is not only qualitative. In our analysis of the stability of fixed points we kept on magnifying the neighborhood

26.1
page 542

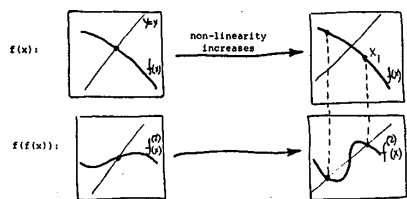


Figure 26.24:

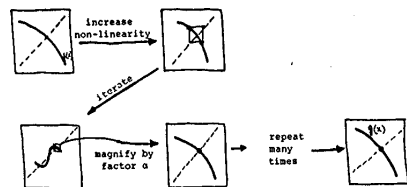


Figure 26.25:

of the fixed point, figure 26.25. The neighborhoods of successive fixed points look very much the same after iteration and rescaling. After we have magnified the neighborhoods of fixed points many times, practically all information about the global shape of the starting function $f(x)$ is lost, and we are left with a *universal function* $g(x)$. Denote by T the operation indicated in figure 26.25 iterate twice and rescale by (without changing the non-linearity parameter),

$$Tf(x) = \alpha f(f(x/\alpha)), \tag{26.5}$$

$g(x)$ is self-replicating under rescaling and iteration, figure 26.26. More precisely, this can be stated as the *universal equation*

$$g(x) = \alpha g(g(-x/\alpha)), \tag{26.6}$$

which determines both the universal function $g(x)$ and $\alpha = -1/g(1) = 2.50290787\dots$, with normalization convention $g(0) = 1$.

Example 26.3 An approximate period doubling renormalization.

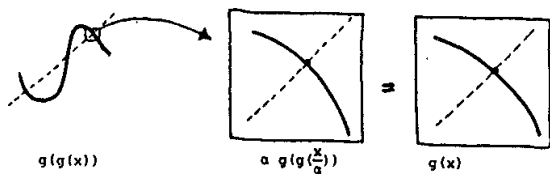


Figure 26.26:

remark, contributor credits to IsaKuz05c; also Hellemann

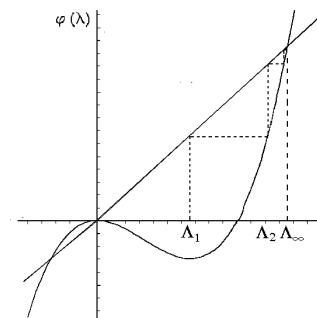


Figure 26.27: Iteration of the approximate renormalization transformation (26.10). Dashed line designates the backward iterations starting at the first period doubling bifurcation point, $\lambda_1 = 3/4$, and mapping to the further bifurcation points λ_m .

As the simplest examples of a period-doubling cascade, consider the map

$$x_{n+1} = f_\lambda(x_n) = \lambda - x_n^2, \quad \lambda, x_n \in \mathbb{R}. \tag{26.7}$$

The two fixed points of f , $x_\pm = \frac{1 \pm \sqrt{1+4\lambda}}{2}$, are the roots of $x_* = \lambda - x_*^2$. At $\lambda = 3/4$ the stability multiplier $\Lambda = f'_\lambda(x_*)$ of the fixed point $x_* = \frac{1+\sqrt{1+4\lambda}}{2}$ is marginal, $\Lambda = -2x_* = -1$. For $\lambda > 3/4$, the fixed point loses its stability and undergoes a period-doubling bifurcation. Values λ for subsequent bifurcations can be found by means of the following approximate renormalization method. Apply the map (26.7) two times:

$$x_{n+2} = \lambda - \lambda^2 + 2\lambda x_n^2 - x_n^4, \tag{26.8}$$

and drop the quartic term x_n^4 . By the scale transformation

$$x_n \rightarrow x_n/\alpha_0, \quad \alpha_0 = -2\lambda, \tag{26.9}$$

this can be rewritten in the form $x_{n+2} = \lambda_1 - x_n^2$, which differs from (26.7) only by renormalization of λ

$$\lambda_1 = \varphi(\lambda) = -2\lambda(\lambda - \lambda^2). \tag{26.10}$$

The map parametrized by λ , approximates two applications of the original map. Repeating the renormalization transformation (26.10) with scale factors $\alpha_m = -2\lambda_m$, one obtains a sequence of the form

$$x_{n+2^m} = \lambda_m - x_n^2, \quad \lambda_m = \varphi(\lambda_{m-1}). \tag{26.11}$$

Fixed points of these maps correspond to the 2^m -cycles of the original map. All these cycles, as well as the fixed point of the map (26.7), become unstable at $\lambda_m = \Lambda_1 = 3/4$. Solving the chain of equations

$$\Lambda_1 = \varphi(\Lambda_2) \quad \Lambda_2 = \varphi(\Lambda_3) \quad \dots \quad \Lambda_{m-1} = \varphi(\Lambda_m), \tag{26.12}$$

we get the corresponding sequence of bifurcation values of parameter λ (with $\lambda \approx \Lambda_m$ the 2^m -cycle of (26.7)). From iteration diagram of figure 26.27 it is evident, that

this sequence converges with $m \rightarrow \infty$ to a definite limit Λ_∞ , the fixed point of the renormalization transformation. It satisfies the equation $\Lambda_\infty = \varphi(\Lambda_\infty)$, thus $\Lambda_\infty = (1 + \sqrt{3})/2 \approx 1.37$. The scaling factors also converge to the limit: $\alpha_m \rightarrow \alpha$, where $\alpha = -2\Lambda_\infty \approx 2.74$. The multipliers (Floquet eigenvalues of the 2^m -cycles) converge to $\mu_m \rightarrow \mu = \sqrt{1 - 4\Lambda_\infty} \approx -1.54$.

From transformation (26.11) on can also describe the convergence of the bifurcation sequence:

$$\Lambda_m = \varphi(\Lambda_\infty) + \varphi'(\Lambda_\infty)(\Lambda_{m+1} - \Lambda_\infty) = \Lambda_\infty + \delta(\Lambda_{m+1} - \Lambda_\infty) \quad (26.13)$$

where the Feigenbaum $\delta = \varphi'(\Lambda_\infty) = 4 + \sqrt{3} \approx 5.73$ characterizes parameter rescaling for each successive period doubling.

The approximate values of Feigenbaum's universal space and parameter scaling constants are reasonably close to the exact values,

	exact	approximate	
α	=	-2.502...	-2.74
δ	=	4.669...	5.73

considering the crudeness of the approximation: the universal fixed-point function $g(x)$ is here truncated to a quadratic polynomial.

(O.B. Isaeva and S.P. Kuznetsov)

If you arrive at $g(x)$ the way we have, by successive bifurcations and rescalings, you can hardly doubt its existence. However, if you start with (26.6) as an equation to solve, it is not obvious what its solutions should look like. The simplest thing to do is to approximate $g(x)$ by a finite polynomial and solve the universal equation numerically, by Newton's method. This way you can compute α and δ to much higher accuracy than you can ever hope to measure them to experimentally.

There is much pretty mathematics in universality theory. Despite its simplicity, nobody seems to have written down the universal equation before 1976, so the subject is still young. We do not have a series expansion for α , or an analytic expression for $g(x)$; the numbers that we have are obtained by boring numerical methods. So far, all we know is that $g(x)$ exists. What has been proved is that the Newton iteration converges, so we are no wiser for the result. In some situations the universal equation (26.6) has analytic solutions; we shall return to this in the discussion of intermittency (SECTION 10). The universality theory has also been extended to iterations of complex polynomials (SECTION 12).

To see why the universal function must be a rather crazy function, consider high iterates of $f(x)$ for parameter values corresponding to 2-, 4- and 8-cycles, figure 26.28. If you start anywhere in the unit interval and iterate a very large number of times, you end up in one of the cycle points. For the 2-cycle there are two possible limit values, so $f(f(\dots f(x)))$ resembles a castle battlement. Note the infinitely many intervals accumulating at the unstable $x = 0$ fixed point. In a bifurcation of the 2-cycle into the

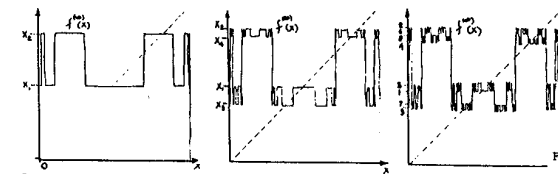


Figure 26.28:

4-cycle each of these intervals gets replaced by a smaller battlement. After infinitely many bifurcations this becomes a fractal (i.e., looks the same under any enlargement), with battlements within battlements on every scale. Our universal function $g(x)$ does not look like that close to the origin, because we have enlarged that region by the factor $\alpha = 2.5029\dots$ after each period-doubling, but all the wiggles are still there; you can see them in Feigenbaum's (1978) plot of $g(x)$. For example, (26.6) implies that if x^* is a fixed point of $g(x)$, so is $\alpha(x^*)$. Hence $g(x)$ must cross the lines $y = x$ and $y = -x$ infinitely many times. It is clear that while around the origin $g(x)$ is roughly a parabola and well approximated by a finite polynomial, something more clever is needed to describe the infinity of $g(x)$'s wiggles further along the real axis and in the complex plane.

All this is fun, but not essential for understanding the physics of the onset of chaos. The main thing is that we now understand where the universality comes from. We start with a complicated many-dimensional dynamical system. A Poincaré map reduces the problem from a study of differential equations to a study of discrete iterations, and dissipation reduces this further to a study of one-dimensional iterations (now we finally understand why the phase-space trajectory in the turbulence experiment undergoes a series of bifurcations as we turn the heat up!). The successive bifurcations take place in smaller and smaller regions of the phase space. After n bifurcations the trajectory splittings are of order $\alpha^{-n} = (0.399\dots)^{-n}$ and practically all memory of the global structure of the original dynamical system is lost (see figure 26.29). The asymptotic self-similarities can be encoded by universal equations. The physically interesting scaling numbers can be quickly estimated by simple truncations of the universal equations, such as example 26.3 (May and Oster 1980, Derrida and Pomeau 1980, Helleman 1980a, Hu 1981). The full universal equations are designed for accurate determinations of universal numbers; as they have built-in rescaling, the round-off errors do not accumulate, and the only limit on the precision of the calculation is the machine precision of the computer.

Anything that can be extracted from the asymptotic period-doubling regime is universal; the trick is to identify those universal features that have a chance of being experimentally measurable. We will discuss several such extensions of the universality theory in the remainder of this introduction.

remark 1978

comment about universal equation

↓PRELIMINARY
make up a example

↑PRELIMINARY

↓PRELIMINARY
↑PRELIMINARY

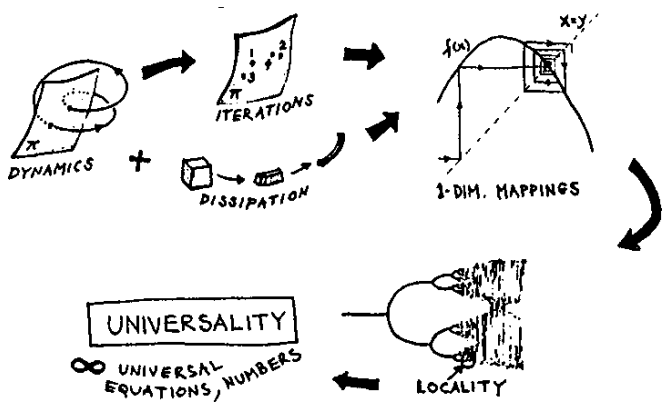


Figure 26.29:

26.5 The unstable manifold

Feigenbaum delta

$$\delta = \lim_{n \rightarrow \infty} \frac{r_{n-1} - r_n}{r_n - r_{n+1}} = 4.6692016 \dots \quad (26.14)$$

is the universal number of the most immediate experimental import - it tells us that in order to reach the next bifurcation we should increase the Rayleigh number (or friction, or whatever the controllable parameter is in the given experiment) by about one fifth of the preceding increment. Which particular parameter is being varied is largely a question of experimental expedience; if r is replaced by another parameter $R = R(r)$, then the Taylor expansion

$$R(r) = R(r_\infty) + (r - r_\infty)R'(r_\infty) + (r - r_\infty)^2 R''(r_\infty)/2 + \dots$$

yields the same asymptotic delta

$$\delta \simeq \frac{R(r_{n-1}) - R(r_n)}{R(r_n) - R(r_{n+1})} = \frac{r_{n+1} - r_n}{r_n - r_{n+1}} + O(\delta^n) \quad (26.15)$$

providing, of course, that $R'(r_\infty)$ is non-vanishing (the chance that a physical system just happens to be parametrized in such a way that $R'(r_\infty) = 0$ is nil).

In deriving the universal equation (26.6) we were intentionally sloppy, because we wanted to introduce the notion of encoding self-similarity by

26.3
page 543

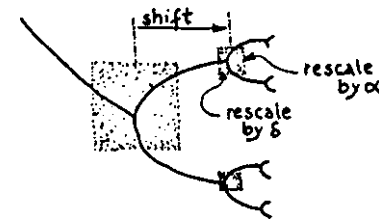


Figure 26.30:

universal equations without getting entangled in too much detail. We obtained a universal equation which describes the self-similarity in the x -space, under iteration and rescaling by α . However, the bifurcation tree figure 26.13 is self-similar both in the x -space and the parameter space: each branch looks like the entire bifurcation tree. We will exploit this fact to construct a universal equation which determines both α and δ .

Let T^* denote the operation of iterating twice, rescaling x by α , *shifting* the non-linearity parameter to the corresponding value at the next bifurcation (more precisely, the value of the nonlinearity parameter with the same *stability*, i.e., the same slope at the cycle points), and *rescaling* it by δ :

$$T^* f_{R_n + \Delta_n p}(x) = \alpha_n f_{R_n + \Delta_n(1+p/\delta_n)}(x/\alpha_n) \quad (26.16)$$

Here R_n is a value of the non-linearity parameter for which the limit cycle is of length 2^n , Δ_n is the distance to R_{n+1} , $\delta_n = \Delta_n/\Delta_{n+1}$, p provides a continuous parametrization, and we apologize that there are so many subscripts. T^* operation encodes the self-similarity of the bifurcation tree figure 26.13, see figure 26.30:

For example, if we take the fish population curve $f(x)$ (26.4) with R value corresponding to a cycle of length 2^n , and act with T^* , the result will be a similar cycle of length 2^n , but on a scale α times smaller. If we apply T^* infinitely many times, the result will be a universal function with a cycle of length 2^n :

$$g_p(x) = (T^*)^\infty f_{R+p\Delta}(x) \quad (26.17)$$

If you can visualize a space of all functions with quadratic maximum, you will find figure 26.31 helpful. Each transverse sheet is a manifold consisting of functions with 2^n -cycle of given stability. T^* moves us across this transverse manifold toward g_p .

$g_p(x)$ is invariant under the self-similarity operation T^* , so it satisfies a universal equation

$$g_p(x) = \alpha g_{1+p/\delta}(g_{1+p/\delta}(x/\alpha)) \quad (26.18)$$

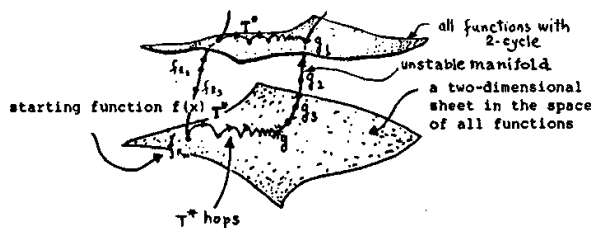


Figure 26.31:

p parameterizes a one-dimensional continuum family of universal functions. Our first universal equation (26.6) is the fixed point of the above equation:

$$p^* = 1 + p^*/\delta \tag{26.19}$$

and corresponds to the asymptotic 2^∞ -cycle.

The family of universal functions parametrized by p is called the *unstable manifold* because T -operation (26.5) drives p away from the fixed point value $g(x) = g_{p^*}(x)$.

You have probably forgotten by now, but we started this section promising a computation of δ . This we do by linearizing the equations (26.18) around the fixed point p^* . Close to the fixed point $g_p(x)$ does not differ much from $g(x)$, so one can treat it as a small deviation from $g(x)$:

$$g_p(x) = g(x) + (p - p^*)h(x)$$

Substitute this into (26.18), keep the leading term in $p - p^*$, and use the universal equation (26.6). This yields a universal equation for δ :

$$g'(g(x))h(x) + h(g(x)) = (\delta/\alpha)h(x) \tag{26.20}$$

We already know $g(x)$ and α , so this can be solved numerically by polynomial approximations, yielding $\delta = 4.6692016\dots$, together with a part of the spectrum of eigenvalues and eigenvectors $h(x)$.

Actually, one can do better with less work; T^* -operation treats the coordinate x and the parameter p on the same footing, which suggests that we should approximate the entire unstable manifold by a double power series

$$g_p(x) = \sum_{j=0}^N \sum_{k=0}^N c_{jk} x^{2j} p^k \tag{26.21}$$

The scale of x and p is arbitrary. We will fix it by the normalization conditions

$$g_0(0) = 0, \tag{26.22}$$

$$g_1(0) = 1, \tag{26.23}$$

$$g_1(1) = 0,$$

The first condition means that the origin of p corresponds to the superstable fixed point. The second condition sets the scale of x and p by the superstable 2-cycle. (Superstable cycles are the cycles which have the maximum of the map as one of the cycle points.) Start with any simple approximation to $g_p(x)$ which satisfies the above conditions (for example, $g(x) = p - x^2$). Apply the T^* -operation (26.16) to it. This involves polynomial expansions in which terms of order higher than M and N in (26.21) are dropped. Now find by Newton's method the value of δ which satisfies normalization (26.23). This is the only numerical calculation you have to do; the condition (26.23) automatically yields the value of α . The result is a new approximation to g_p . Keep applying T^* until the coefficients in (26.21) repeat; this has moved the approximate g_p toward the unstable manifold along the transverse sheets indicated in figure 26.31. Computationally this is straightforward, the accuracy of the computation is limited only by computer precision, and at the end you will have α , δ and a polynomial approximation to the unstable manifold $g_p(x)$.

As δ controls the convergence of the high iterates of the initial mapping toward their universal limit $g(x)$, it also controls the convergence of most other numbers toward their universal limits, such as the scaling number $\alpha_n = \alpha + O(\delta^{-n})$, or even δ itself, $\delta_n = \delta + O(\delta^{-n})$. As $1/\delta = 0.2141\dots$, the convergence is very rapid, and already after a few bifurcations the universality theory is good to a few per cent. This rapid convergence is both a blessing and a curse. It is a theorist's blessing because the asymptotic theory applies already after a few bifurcations; but it is an experimentalist's curse because a measurement of every successive bifurcation requires a fivefold increase in the experimental accuracy of the determination of the non-linearity parameter r .

↓PRELIMINARY

26.6 Cookie-cutter's universality

Refs. [18.2, 18.6]: cycle expansion for δ .

Ref. [26.11]: method for computation of the generalized dimensions of fractal attractors at the period-doubling transition to chaos, via an eigenvalue problem formulated in terms of functional equations, with a coefficient expressed in terms of Feigenbaum's universal fixed-point function.

↑PRELIMINARY

Commentary

Remark 26.1 Sources. This chapter is based on a Nordita lecture prepared together with Mogens Høgh Jensen (Cvitanović and Høgh Jensen 1982). Ulla Selmer prepared the drawings, Oblivia Kaypro stood for initial execution.

The universal equation (26.6) was formulated by P. Cvitanović in March 1976, in collaboration with M.J. Feigenbaum [26.2]. Equation (26.19) is not necessarily the only way to formulate universality. Coulet and Tresser [26.5] have proposed similar equations, after Feigenbaum's work became known, but before Joel Lebowitz rescued him from the referees and arranged for its publication. Daido (1981a) has introduced a different set of universal equations.

find Hoppensteadt
(1978)

We recommend review by May [26.6]

If $f(x)$ is not quadratic around the maximum, the universal numbers will be different - see Villela Mendés (1981) and Hu and Mao (1982b) for their values. According to Kuramoto and Koga (1982) such mappings can arise in chemical turbulence.

The elegant unstable manifold formulation of universality (26.18) is due to Vul and Khanin (1982) and Goldberg, Sinai and Khanin (1983).

Derrida, Gervois and Pomeau (1979) have extracted a great many metric universalities from the asymptotic regime. Grassberger (1981) has computed the Hausdorff dimension of the asymptotic attractor. Lorenz (1980) and Daido (1981b) have found a universal ratio relating bifurcations and reverse bifurcations.

A nice description of initial experiments has been given by Libchaber and Maurer(1981). The most thorough exposition available is the Collet and Eckmann [26.4] monograph. We also recommend Hu (1982), Crutchfield, Farmer and Huberman (1982), Eckmann (1981) and Ott (1981).

Collet and Eckmann (1980a) and Collet, Eckmann and Koch (1980) give a detailed description of how a dissipative system becomes one-dimensional.

The period route to turbulence that we describe is by no means the only one; see Eckmann (1981) discussion of other routes to chaos.

The geometric parameter convergence was first noted by Myrberg (1958), and independently of Feigenbaum, by Grossmann and Thomae (1977). These authors have not emphasized the universality of δ .

Refs. [26.9, T.5, 26.10] are interesting; they compute solutions of the period-doubling fixed point equation using methods of Schöder and Abel, yielding what are so far the most accurate δ and α .

The theory of period-doubling universal equations and scaling functions is developed in Kenway's notes of Feigenbaum 1984 Edinburgh lectures [26.3] (trifle hard to track down).

A nice discussion of circle maps and their physical applications is given in refs. [28.3] The universality theory for golden mean scalings is developed in refs. [?, 28.7, 28.14] The scaling functions for circle maps are discussed in ref. [28.4].

⇓PRELIMINARY

Remark 26.2 Universality theory for conservative systems. The details of the universality theory are different for dissipative and conservative systems; however, the spirit is the same. Almost all that we shall say applies to dissipative systems we will not discuss conservative systems, but refer the reader to ???.

↑PRELIMINARY

⇓PRELIMINARY

Résumé

References

[26.1] M. J. Feigenbaum, "Quantitative Universality for a Class of Non-Linear Transformations," *J. Stat. Phys.* **19**, 25 (1978).

[26.2] M. J. Feigenbaum, *J. Stat. Phys.* **21**, 669 (1979); reprinted in ref. [18.5].

[26.3] M.J. Feigenbaum and R.D. Kenway, in *Proceedings of the Scottish Universities Summer School* (1983).

[26.4] P. Collet and J.P. Eckmann, *Iterated maps on the interval as dynamical systems* (Birkhauser, Boston 1980).

[26.5] P. Coulet and C. Tresser, "Itérations d'endomorphismes et groupe de renormalisation," *J. Phys. Colloque C* **539**, 5 (1978); *C.R. Acad. Sci. Paris* **287A**, 577 (1978).

[26.6] R. May, "Simple mathematics models with very complicated dynamics," *Nature* **261**, 459 (1976).

[26.7] M. Pollicott, "A Note on the Artuso-Aurell-Cvitanović approach to the Feigenbaum tangent operator," *J. Stat. Phys.*, **62**, 257 (1991).

[26.8] Y. Jiang, T. Morita and D. Sullivan, "Expanding direction of the period doubling operator," *Comm. Math. Phys.* **144**, 509 (1992).

[26.9] K.M. Briggs, "A precise calculation of the Feigenbaum constants," *Math. of Computation*, 435 (1991).

[26.10] K.M. Briggs, T.W. Dixon and G. Szekeres, "Analytic solutions of the Cvitanović-Feigenbaum and Feigenbaum-Kadanoff-Shenker equations," *Internat. J. Bifur. Chaos* **8**, 347 (1998).

[26.11] S.P. Kuznetsov and A.H. Osbaldestin, "Generalized dimensions of Feigenbaum's attractor from renormalization-group functional equations," nlin.CD/0204059.

[26.12] "Feigenbaum Constant," mathworld.wolfram.com/FeigenbaumConstant.html.

[26.13] "Feigenbaum Function," mathworld.wolfram.com/FeigenbaumFunction.html.

[26.14] O.B. Isaeva and S.P. Kuznetsov, "Approximate description of the Mandelbrot Set. Thermodynamic analogy," nlin.CD/0504063. *Nonlinear Phenomena in Complex Systems* **8**, 157 (2005).

[26.15] C. McMullen, "Complex dynamics and renormalization" (Princeton Univ. Press, 1994).

⇓PRELIMINARY

[26.16] D. Smania “On the hyperbolicity of the period-doubling fixed point,”
from *Trans. Amer. Math. Soc.* **358**, 1827 (2006).

[26.17] F. Moon, *Chaotic oscillations*

[26.18] A.Yu. Kuznetsova, A.P. Kuznetsov, C. Knudsen, E. Mosekilde. Catastrophe theoretic classification of nonlinear oscillators, *Int. J. of Bifurcations and Chaos*, V.12, No 4, 2004, P. 1241-1266.

↑PRELIMINARY